Eur. Phys. J. D **6**, 193–200 (1999)

THE EUROPEAN PHYSICAL JOURNAL D

EDP Sciences

Saturation spectroscopy of the A-X transition of the ICl molecule

G. Bazalgette, M. Büchner, C. Champenois, G. Trenec, and J. Vigué[a]

Laboratoire Collisions Agrégats Réactivité, I.R.S.A.M.C., University Paul Sabatier
and CNRS U.M.R. 5589 118, route de Narbonne, 31062 Toulouse Cedex, France

Received: 27 July 1998 / Received in final form: 30 November 1998

Abstract. We describe the first saturation spectroscopy experiment concerning the A-X transition of ICl with considerably better resolution than previous works. Form our data, improved constants for the hyperfine structure of the excited state are determined. The A-X transition of ICl could be used to develop a set of secondary frequency standards and its metrologic qualities are discussed.

PACS. 33.15.Pw Fine and hyperfine structure – 33.80.Wz Other multiphoton processes

1 Introduction

We describe a very high resolution experiment on the A-X transition of ICl. By saturating this very weak transition, we have achieved a tenfold improvement in resolution over that observed from the residual Doppler broadening present in our molecular beam. The interest of this work is twofold:

- The increased resolution improves the accuracy of hyperfine constants in the excited state. Since the development of microwave spectroscopy [1], the molecular hyperfine structure is known to carry important information on the occupation of the outer electronic shell. It was shown around 1980 that these ideas can be given a more quantitative form in the case of the I_2 molecule [2] and the recent measurements on ICl have extended this type of analysis [3–7].
- Various circumstances make favorable the saturation of this very weak and intrinsically very narrow transition ($\tau = 430 \pm 30$ μs [8], $\Delta\nu \approx 370$ Hz), which should lead to a set of secondary optical frequency standards - lines 400 - fold sharper than those due to Doppler-free iodine.

The content of this paper is the following: we review first the knowledge of the A-X transition of ICl (see Sect. 2) and we describe in Section 3 the experimental setup. The signals are presented and analyzed in Section 4. The metrologic interest of these transitions is discussed in Section 5. Some concluding remarks are presented in Section 6.

[a] e-mail: jacques@yosemite.ups-ttlse.fr

2 The A-X transition of ICl

2.1 The spectroscopy of the levels on the $A^3\Pi_1$ and $X^1\Sigma^+$ states

The spectroscopy of the A-X transition has been the subject of several studies by Coxon and co-workers [9,10]. The lowest vibrational levels of the X state are very accurately known thanks to IR Fourier spectroscopy [11]. The ground state hyperfine structure has been measured very accurately with microwave spectroscopy by Herbst and Steinmetz [12]. Finally, several studies made by Janda and co-workers [3,4,6,7] have given excellent knowledge of the A state hyperfine structure: these studies have also provided accurate values of the band origins of the A-X system and of the A state rotational constants. As a result, for the low J lines that can be observed in a supersonic beam of ICl, we can calculate with great accuracy their positions and also their hyperfine structures. Therefore, the assignment of the observed lines is straightforward.

Let us review briefly the understanding of the hyperfine structure of the A and X states. Until now, this hyperfine structure has been very satisfactorily described by the simple Hamiltonian:

$$H = \sum_{k=1,2} \sum_{i=\mathrm{I,Cl}} H_k(i)\,. \qquad (1)$$

In this expression, the $k = 1$ terms are the magnetic dipolar interactions and the $k = 2$ terms are the electric quadrupolar interactions. The detailed forms of these terms will not be recalled here (see [3,4,6,7,12]). The hyperfine terms involving the chlorine nucleus are typically 10 times smaller than those involving the iodine nucleus. As a consequence, the hyperfine structure is almost diagonal in the $|\mathbf{J}, \mathbf{I}_1, \mathbf{F}_1, \mathbf{I}_2, \mathbf{F}\rangle$ basis set in the high-J limit, and this is a good approximation for the $J = 8$ or 9 levels studied here. $\mathbf{I}_1$ and $\mathbf{I}_2$ are the nuclear spins of the iodine

($I_1 = 5/2$) and chlorine ($I_2 = 3/2$) nucleus. We will note $m_1 = F_1 - J$ and $m_2 = F - F_1$, and m_1 and m_2 are the projections of the two nuclear spins on **J**, in the high-J limit. In this limit, the transitions approximately follow the selection rules:

$$\Delta F_1 = \Delta F = \Delta J = 0, \pm 1 \,.$$

These rules can be restated in the form

$$\Delta m_1 = \Delta m_2 = 0 \,.$$

As a consequence of these selection rules, the hyperfine structure of a line is made of only $(2I_1+1)\times(2I_2+1) = 24$ main components. Because of the conservation of m_1 and m_2, their values are used to label the lines in the spectra.

The scalar and tensor spin-spin interactions between the two nuclear magnetic dipole moments have been neglected in all previous studies of ICl A and X states. Comparison with the case of the iodine molecule suggests that this might not be fully justified, especially in the A state [13–16]. However, the limited accuracy of our laser frequency measurements prevents us from introducing this refinement.

2.2 The transition dipole moment

The magnitude of the transition dipole moment is very important for the feasibility of a saturation experiment. This quantity $\langle Av'|\mu|Xv''\rangle$ is approximately given by:

$$\langle Av'|\mu|Xv''\rangle = \langle v'|v''|\rangle \mu_{\mathrm{AX}} \,, \qquad (2)$$

where the dependence on internuclear distance has been neglected. This approximation is not very good for the visible system of halogen molecules, because the transition moments must vanish for large internuclear distances when the molecule dissociates into ${}^2\mathrm{P}_J + {}^2\mathrm{P}_{J'}$ atoms. This is well established for the B-X transition moment of the I_2 molecule [17–19]. Unfortunately, for the A-X transition of ICl, the available information is rare and not very precise, and this prevents any refinement.

The value of μ^2_{AX} can be deduced from several absorption studies and from the measured radiative decay rate Γ_{rad}. The value due to Cummings [20] was deduced from photographic measurements of resolved absorption lines and its large error bar is largely due to the photographic technique. Harris *et al.* [8] have made a measurement of the unresolved absorption near 600 nm and a measurement of the radiative decay rate of the level $Av' = 18$. Their paper gives the necessary σ^3 average for this vibrational level (where σ is the wave number of the emission lines, each line being weighted by its Franck Condon factor) so that the evaluation of μ_{AX} from the radiative decay rate is straightforward. Finally, we have reanalyzed [21] the absorption data of Seery and Britton [22] using the Sulzer and Wieland equation [23] and we have deduced from this analysis a new determination of μ^2_{AX}. These four values of μ^2_{AX} are collected in Table 1 and are in reasonably good agreement. We will accept $\mu^2_{\mathrm{AX}} = (1.0 \pm 0.3) \times 10^{-2} D^2$.

Table 1. This table collects four independent measurements of the A-X transition dipole moment μ^2_{AX}.

Source	Technique	$\mu^2_{\mathrm{AX}}(D^2)$
Cummings[a]	Resolved absorption	$(23^{+23}_{-11}) \times 10^{-3}$
Harris *et al.*[b]	Unresolved absorption near 600 nm	8.6×10^{-3}
Haris *et al.*[b]	Lifetime neasurement	$(13 \pm 1) \times 10^{-3}$
Seery and Britton[c]	Unresolved absorption	6.0×10^{-3}

[a] From reference [20];
[b] from reference [8];
[c] new analysis of their data [22] made by one of us [21].

Coxon has calculated the A-X Franck-Condon factors [9]. The present work concerns only the $v' = 21$–$v'' = 0$ transition, with a value $|\langle v' = 21|v'' = 0\rangle|^2 = 0.01705$. The variation with v' is rather slow and all the levels $11 \leq v' \leq 31$ satisfy $|\langle v'|v'' = 0\rangle|^2 \geq 0.005$, so that many vibrational bands of the A-X system provide transitions of comparable strengths.

2.3 The Zeeman and Stark effects

We have done our experiment without any efforts to cancel ambient electric and magnetic fields. It is therefore important to consider the Zeeman and Stark effects as they can play a role in the linewidth and shape.

A precise calculation of the Zeeman effect splitting requires the coupling of nuclear spins, but the order of magnitude can be obtained while neglecting their existence. The X state has a weak paramagnetic character which can be neglected relative to the strong paramagnetic character of the A ${}^3\Pi_1$ state. The A state rotational Landé factor is [24]

$$g_J = \frac{\Omega(\Lambda + 2\Sigma)}{J(J+1)} = \frac{1}{J(J+1)} \,. \qquad (3)$$

The splitting between the extreme Zeeman components of a line is given by

$$\Delta\nu = (2J+1) g_J \mu_{\mathrm{B}} B/h. \qquad (4)$$

For the $J \approx 10$ levels which are used in our experiment, the order of magnitude of this splitting is $\Delta\nu \approx 100$ kHz for the Earth's magnetic field ($B = 4 \times 10^{-5}$ T). This could be easily reduced well below 1 kHz by canceling the field within 0.1 μT. This cancellation should be rather easily done as it must be achieved only for the very small intersection of the laser beam and of the molecular beam.

In low field, the Stark effect is stronger in the A state than in the X state because, in the A state, the e/f levels with opposite parities are quasi-degenerate. The A state dipole moments are known since the work of Cummings

and Klemperer [25], and very accurate values are now available [26]: for instance, $\mu_A(v'=21) = 1.049 \pm 0.003$D. The order of magnitude of the low field Stark effect is given by

$$\delta E_{\text{Stark}} \approx \frac{\mu_A^2 E^2}{h\Delta_{ef}}, \tag{5}$$

where $h\Delta_{ef}$ is the energy to the nearest opposite parity level and E is the electric field. The Λ-doubling constant in the A $v'=21$ level is small ($q = 3.95(17) \times 10^{-5}\text{cm}^{-1}$ [9], $q = 7.47(20) \times 10^{-5}\text{cm}^{-1}$ [7]). For a level with J close to 10, the splitting Δ_{ef} between the e- and f-party sublevels is calculated to be $\Delta_{ef} \approx$ 100-200 MHz. The hyperfine contributions are comparable with or even larger than this estimate. The resulting order of magnitude of the Stark effect is given by $\delta E_{\text{Stark}}/h(\text{Hz}) \approx 0.3 \times [E(\text{V/m})]^2$. For typical stray electric fields of a few volts/meter, this contribution to the linewidth is negligible.

3 Experimental setup

3.1 Laser system

We use a tunable ring dye laser following F. Biraben's design [27] pumped by a Spectra Physics Ar^+ laser (model 2015 S). The dye is Rhodamine 6G and we obtain reliably a 600 mW power for a 5 W pump power at 515 nm. The laser frequency is locked to the resonance frequency of a Fabry-Perot cavity, following the Hänsch Couillaud design [28]. We have optimized the electronic design of our servo loop following the ideas developed by G. Camy [29]. The linewidth due to residual frequency jitter has been estimated to be 700 kHz by using a high finesse Fabry-Perot interferometer (finesse $\approx$ 3000, free spectral range 500 MHz).

Because the saturation signals are weak, the laser frequency is swept slowly, typically at 10 kHz/s over a width of 30-50 MHz. In order to minimize drifts of the invar Fabry-Perot cavity, its temperature was controlled to 10^{-2}°C by a proportional integral and differential servo loop, and its ambient pressure was controlled by placing it within a vacuum-tight (but not evacuated) container. We have not observed any problems due to pressure fluctuations.

3.2 Frequency measurement

Our home made lambdameter of classic design [30,31] gives the laser frequency to approximately 100 MHz. In order to calibrate the laser scans, we needed a stable frequency marker. We used a Fabry-Perot interferometer made from invar thermally compensated with copper, situated in a vacuum chamber evacuated by an ion pump (residual pressure close to 10^{-6}mbar. The temperature of the vacuum chamber was controlled by water circulation to $\pm 10^{-2}$°C. The mirrors used have a high reflectivity $R = 99.9\%$ at 600 nm and thus provide a high finesse ($F = 3000$). The mirrors were separated by $L = 0.4935$ m, and the radii of curvature were $R_1 = \infty$ and $R_2 = 1.5$ m. With this choice of radii of curvature, the Fabry-Perot interferometer is not degenerate [32] and the transmission peaks $TEM_{mn}(N)$ have a frequency

$$\nu_{N,m,n} = \frac{c}{2L}[N + 1 + (m+n+1)\phi_0], \tag{6}$$

with $\phi_0 = 0.1944$ and $c/2L = 303.88$ MHz. The modes $N, (m+n)$ and the modes $N+1, (m+n-5)$ are separated by 8.51 ± 0.01 MHz, which gives the needed frequency markers. Because of various minor defects, the remaining degeneracy of the transverse modes is not exact and the peaks are broader than the value predicted from the cavity finesse and the laser frequency jitter.

3.3 The molecular beam

We have already described our ICl molecular beam (see our previous works on the Stark spectra of the A-X transition of ICl [33]). The original part of this design is that the fluorescence is not detected in the excitation region but nearly 200 mm downstream, an arrangement made possible by the long lifetime of ICl A state. This trick is very efficient at reducing stray laser light. The distance from nozzle to excitation region has been reduced to 35 mm, and the nozzle diameter has been increased to 170 μm, while the ICl pressure was slightly reduced to 13 mbar. These modifications have increased the LIF signal by a factor close to 10, with typical count rates of 10^5 detected photons/second.

3.4 LIF and saturation arrangements

We excite the molecular beam with either one laser beam or two counterpropagating laser beams. In both cases, the laser beams are perpendicular to the molecular beam:

- With the single beam arrangement, we record laser-induced fluorescence spectra with a resolution limited by the effective collimation of our molecular beam. The residual Doppler broadening is well represented by an 8 MHz FWHM Gaussian lineshape. Such a spectrum is presented in Figure 1.
- The two-beam arrangement is a realization of the intermodulated fluorescence technique introduced by Sorem and Schwlow [34]. We align the beams so that they counterpropagate; we estimate that this alignment is correct within 0.5 mrad. The two beams are modulated by separate mechanical choppers at $\nu_1 = 601$ Hz and $\nu_2 = 63$ Hz. A synchronous detection (EG&G, model 7220) tuned to ν_1, with the minimum time constant (640 μs), detects the modulated part of the fluorescence signal, and its output is sent to a second synchronous detection (EG&G, model 5209) tuned to ν_2 and operated with a 3 or 10 s time constant. The output of the second synchronous detection is a measurement of the non-linear part of the fluorescence signal.

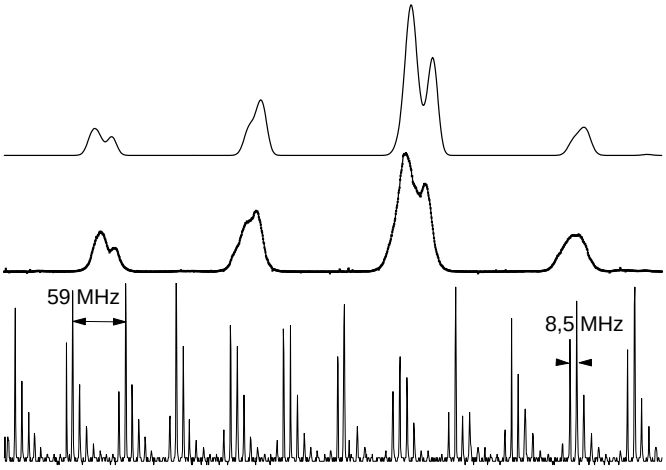

Fig. 1. *Top*: numerical simulation of the band head of the A-X $v' = 21 \leftarrow 0$ transition of ICl (actually a part of the $R(2)$ transition) using the published hyperfine constants [7,12]. This simulation takes into account the broadening due to the residual Doppler effect, using a convolution with an 8 MHz FWHM Gaussian curve. *Center*: laser-induced fluorescence spectrum recorded in a single beam configuration. *Bottom*: transmission peaks of the Fabry-Perot interferometer used as frequency marker. Its free spectral range, $c/2L \approx 303.88$ MHz is separated into 5 parts of about 59 MHz and in each part, the peaks are separated by 8.51 MHz.

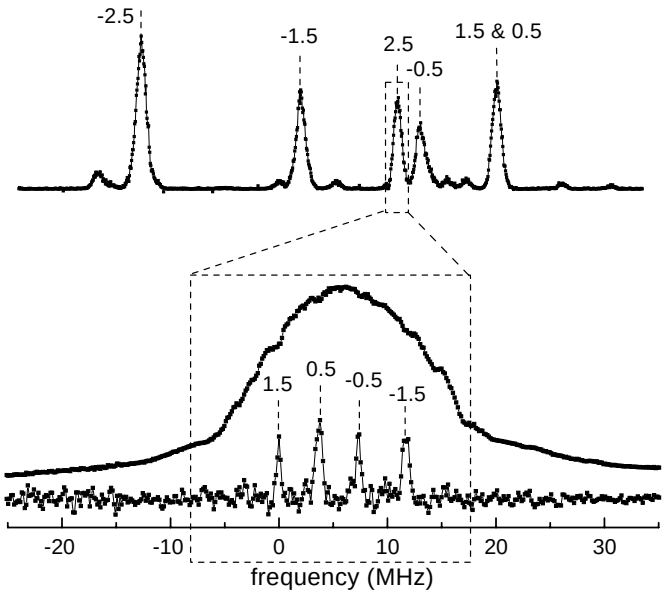

Fig. 2. *Top*: laser-induced fluorescence spectrum of the A-X 21–0 $Q(8)$ transition of ICl, recorded in the single laser beam configuration. The frequency step is about 500 kHz. The hyperfine structure due to the nuclear spin of iodine is well resolved. *Center*: LIF spectrum realized with the two-laser-beam configuration but with a single synchronous detection and the fluorescence dips due to saturation appear weakly. The frequency step is about 200 kHz. The spectrum corresponds to the hyperfine transition labeled by $m_1 = 2.5$. *Bottom*: intermodulated fluorescence spectrum recorded in the same conditions as the previous one but with the two synchronous detections. The hyperfine structure due to the nuclear spin of chlorine is fully resolved and the 4 main components of the $m_1 = 2.5$ line are labeled by their m_2 values.

This arrangement gives a signal very similar to saturated absorption spectroscopy, but it is well adapted to very weak absorption. We were careful to run the photomultiplier (Hamamatsu R943-02) in a linear regime; otherwise, the saturation signals appear on a background due to the non-linearities of the fluorescence detection system. We show in Figure 2 a typical spectrum. Because of the limited length of our laser scans, we have recorded only the structures of the lines that were unresolved in the linear fluorescence spectrum.

4 The signal and its analysis

We have focused our experiments on two rotational transitions belonging to the A-X 21-0 band, namely the $Q(8)$ and $R(8)$ lines. The linear fluorescence spectra are made of a group of 6 main lines corresponding to the selection rule $\Delta F_1 = \Delta J$, where F_1 spans the range $J-5/2$, $J+5/2$. The large hyperfine splittings are due to the iodine nucleus. Then each of these 6 lines is made of 4 main components due to the hyperfine structure of chlorine nucleus. These small splittings are resolved only in our saturation experiment. In their experiments, K. C. Janda an his coworkers were able to resolve this hyperfine structure only for very low J transitions [7], since the magnetic dipolar part of this structure, due to the A state, shrinks when J increases. We show in Figure 3 three examples of resolved structures.

Using the frequency markers given by the Fabry-Perot interferometer, we can calibrate the spectra and measure the splittings. Table 2 gives their measured values after averaging over several similar recordings. This averaging procedure gives information on the reproducibility of our measurements; this information appears in Table 2 as the 1σ error bar.

We have calculated the hyperfine splittings with the constants fitted by K. C. Janda and coworkers [7] (see Tab. 2). This calculation is quite sufficient to explain and assign the observed structures but some discrepancies appear, proving that these constants can be improved.

The two transitions $R(8)$ and $Q(8)$ sample A state levels of opposite parity. The hyperfine structures of the upper levels in these two transitions arise from different combinations eQq_{eff} of the two quadrupolar coupling constants eQq_0 and eQq_2:

$$eQq_{\text{eff}} = eQq_0 \left(\frac{6}{J'(J'+1)} - 2 \right) \pm eQq_2 \,, \qquad (7)$$

where J' is the rotational quantum number of the A state and the $+/-$ sign corresponds to the f/e parity. In the following analysis, the ground state hyperfine constants were fixed to accurate values measured with electric resonance techniques.

Table 2. Some hyperfine splittings measured on the A-X 21-0 $R(8)$ and $Q(8)$ lines. The spectrum has been calibrated with the frequency scale given by the Fabry-Perot interferometer (cf. Fig. 1) and the error bars are deduced from a series of similar recordings. The transitions are labeled by $m_1 = F_1 - J$ and $m_2 = F - F_1$. The transition $m_2 = 1.5$ has been chosen as the origin. The experimental splittings are compared to those calculated using the hyperfine constants fitted by Western *et al.* [7] (Calculation 1) and to the present fit with the constants given in Table 4 (Calculation 2). The agreement between the experimental data and the numerical simulation is clearly better in the second case.

Line	$m_1 = F_1 - J$	$m_2 = F - F_1$	Experimental (MHz)	Calculation 1 (MHz)	Calculation 2 (MHz)
$R(8)$	2.5	1.5	0	0	0
		−1.5	9.69 ± 0.03	7.7	8.87
		0.5	20.44 ± 0.07	17.94	20.21
		−0.5	22.18 ± 0.08	19.18	21.67
$Q(8)$	−0.5	1.5	0	0	0
		0.5	4.25 ± 0.35	3.26	4.28
		−0.5	6.89 ± 0.30	5.92	7.22
		−1.5	19.22 ± 0.27	18.16	19.59

Table 3. Fitted values of the chlorine hyperfine constants a_{Cl} and $eQq_{\mathrm{eff}}(\mathrm{Cl})$ of the A $v' = 21$ state of ICl. The fit has been realized using a linear regression technique on a set of 9 experimental splittings for the $Q(8)$ transition and 12 experimental splittings for the $R(8)$ transition. We compare the present values of $eQq_{\mathrm{eff}}(\mathrm{Cl})$ to those deduced from the results of Western *et al.* [7] (the corresponding 1σ error bars are calculated from the published 1σ error bars of the two quantities $eQq_0(\mathrm{Cl})$ and $eQq_2(\mathrm{Cl})$, assuming a vanishing correlation between the two measurements).

	$R(8)$	$Q(8)$	Source
a_{Cl}(MHz)	-41.6 ± 0.9	-34.7 ± 0.7	Present work
$eQq_{\mathrm{eff}}^{\mathrm{Cl}}$(MHz)	37.5 ± 2.1	175.3 ± 2.0	Present work
$eQq_{\mathrm{eff}}^{\mathrm{Cl}}$(MHz)	51.8 ± 1.8	179.6 ± 1.8	Western *et al.*

We give in Table 3 the best fit for the chlorine hyperfine constants a_{Cl}, measuring the magnetic dipolar interaction and the effective quadrupolar coupling constants $eQq_{\mathrm{eff}}(\mathrm{Cl})$. Comparing our results to those of Janda and co-workers [7] suggests a significant correction of the effective quadrupolar constant for the $eJ' = 9$ level. However, the calculated splittings deduced from the new constants are not in perfect agreement with the experimental ones. Moreover, the magnetic dipolar constant a_{Cl} we deduce from the fit is different for the two parity levels. We are unable to explain this result, since previous experiments gave a unique and very accurate value for a_{Cl}. One possible reason for these discrepancies would be that our measurement of the laser frequency is not of sufficient accuracy. The ideal technique would be to work in the frequency domain by recording the beat frequency between our laser and another laser having its frequency stabilized on some nearby reference line.

Table 4. Chlorine hyperfine constants of the A $v' = 21$ level of ICl deduced from the present work, compared to the chlorine hyperfine constants given by Janda and co-workers [7]

	Present work	Western *et al.*
a_{Cl}(MHz)	-38.1 ± 3.5	33.34 ± 0.30
$eQq_0\mathrm{Cl}$(MHz)	-55.3 ± 0.8	-60.1 ± 1.5
$eQq_2\mathrm{Cl}$(MHz)	69.4 ± 1.4	64.4 ± 2.1

Finally, in Table 4, we give the three chlorine hyperfine constants deduced from the present work and compare them to previously published values. The differences between the new and previous values for $eQq_0(\mathrm{Cl})$ and $eQq_2(\mathrm{Cl})$ are considered meaningful, although they agree within 3 times the cumulated 1σ error bars of the two measurements.

5 Discussion of the interest of the ICl A-X transition for laser frequency secondary standards

5.1 General considerations

The need for laser frequency secondary standards is still very strong as the measurement of a laser frequency by comparison to an atomic clock is not a simple experiment. A list of secondary standards is given for instance by CIPM reports [35], and many other experiments are made to develop such standards. In the long term, it seems clear that the best standards will be given by laser-cooled atoms or ions (see, for instance, [36–38]), but such experiments are still quite challenging and provide only a few lines.

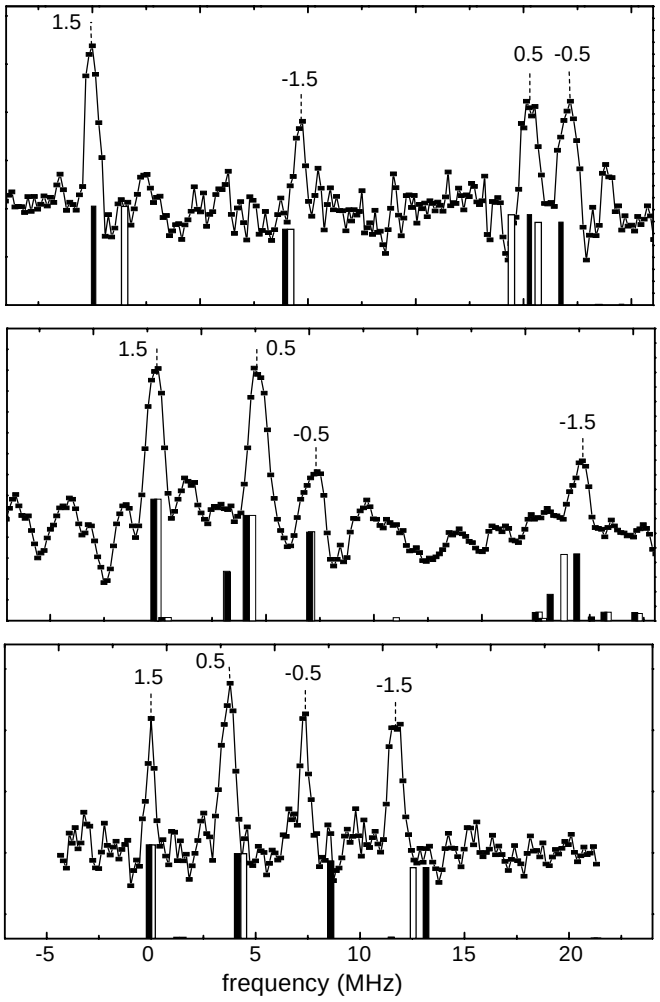

Fig. 3. Intermodulated fluorescence spectrum of the A-X $v' = 21 \leftarrow 0$ $R(8)m_1 = 2.5$ (top), $Q(8)m_1 = -0.5$ (center), $Q(8)m_1 = 2.5$ (bottom) lines of ICl. The experimental spectra are compared to two numerical simulations: the white bars represent the simulation using Western *et al.* [7] constants; the black bars represent the simulation with our final set of chlorine hyperfine constants (cf. Tab. 4). A better agreements is obtained if one uses different constants for the $R(8)$ and $Q(8)$ lines as given in Table 3.

By contrast, the ICl A-X system can provide many lines in the 590-700 nm range, and the ultimate width of these lines is considerably smaller than the commonly used lines belonging to the iodine B-X system. It is our conviction that only very few molecular species can provide a transition in the visible range with as favorable properties as the ICl A-X system.

5.2 Contributions to the linewidth

Many different effects contribute to our observed linewidth. We shall discuss these contributions and the associated limits in an optimized experiment.

Laser jitter

In the present experiment, the frequency jitter is the dominant contribution. We have made some attempts to reduce this frequency jitter below 700 kHz. Problems with our electronics prevented implementation of the Bewster Hall frequency stabilization technique [39,40], a technique with the potential to reduce frequency jitter to near 1 kHz.

Transit time broadening

The transit time of the molecules crossing the laser beam is another important contribution to the linewidth. In the same class of effects, one finds problems associated with the curvature of the laser beam wavefronts and misalignments. These last effects can be reduced by proper alignment but the transit time broadening depends only on the laser waist radius w_0 and on the molecular beam mean velocity u calculated to be $u \approx 330$ m/s. For a waist $w_0 \approx 1$ mm, this broadening is about

$$\Delta\nu = \frac{u}{\pi w_0} \approx 100 \text{ kHz}\,. \tag{8}$$

Without modifying the saturation regime, one can expand the laser beam. It is reasonable to use laser beams with w_0 up to 10 mm, for which the associated broadening would be reduced to the 10 kHz range.

Recoil effect and second-order Doppler effect

The recoil of the molecule due to the photon momentum splits the lines into two components separated by

$$\delta\nu = \frac{h}{m\lambda^2} \approx 7 \text{ kHz}\,, \tag{9}$$

where λ is the laser wavelength and m the molecular mass. This effect has been observed in saturation spectroscopy, even in the visible region [41], but it is very difficult to resolve this doublet. The second-order Doppler effect in a supersonic beam induces little broadening, as the velocity dispersion is small, but it does cause a small shift of the line

$$\delta\nu = \frac{u^2}{2c\lambda} \approx 0.3 \text{ kHz}\,. \tag{10}$$

Interaction with electromagnetic fields

The Stark and Zeeman effects were discussed above, and here we discuss saturation effects. The Rabi frequency Ω is defined by the relation

$$\hbar\Omega = \frac{1}{2\sqrt{2}}\langle v'|v''\rangle \mu_{\text{AX}} E_0\,, \tag{11}$$

where the first factor is the average of $3J$ coefficients over the Zeeman components in the case of a Q transition and linear polarization. E_0 is the laser electric field ($E_0^2 = 4\mu_0 cP/\pi w_0^2$ for a Gaussian laser beam of power P). For

the transitions we studied, we estimate the Rabi frequency for a power $P = 0.3$ W to be

$$\Omega = 1.7 \times 10^6 \mathrm{s}^{-1} .$$

This is a large value and surely gives an important contribution to the observed linewidth. The product of the Rabi frequency by the transit time through the laser beam is of the order of 10. In our experiment, this strong saturation regime was necessary in order to enhance the signal which suffers a considerable dilution due to the laser frequency jitter. With a better laser, the experiment could be made with considerably lower laser power.

Collisional broadening

The intensity of our supersonic beam has been estimated [42]:

$$\mathcal{I} = 10^{18} \text{ molecules/s sr} ,$$

and recent modifications should not modify this by more than a factor of 2. In the excitation volume at a distance $z = 35$ mm from the nozzle, the total ICl density is

$$n_{\mathrm{ICl}} = \frac{\mathcal{I}}{uz^2} \approx 3 \times 10^{18} \mathrm{m}^{-3} . \qquad (12)$$

At such a density, with a polar molecule like ICl, we may fear the effect of the long-range interactions. The general theory of line broadening should be valid [43], and in this case, theory predicts a linewidth the order of 10 MHz for a perturber pressure equal to 1 mbar at 300 K. For the above density, this leads to a broadening in the 1 kHz range. A simple calculation [44] assuming that the dipole does not rotate during the collision predicts the same order of magnitude, near 5 kHz. Such values are acceptable as this would not substantially broaden the lines, but there is also a transition shift associated with this collision process. This shift, which is usually a fraction of the broadening, may be a problem, as it is not easy to control the molecular density in the beam.

6 Concluding remarks

In this paper, we have described the first saturation experiment performed on the A-X system of ICl. Although our experiment is far from optimized, we have demonstrated the feasibility of saturation spectroscopy on this weak molecular transition. Moreover, analysis of the experimental signals has provided a slight improvement of the quadrupolar constants describing the hyperfine interaction of the chlorine nucleus in the A $v' = 21$ level. Using the best laser techniques it would be possible to achieve highly accurate hyperfine constants for the A state. This would be interesting, as the hyperfine constants of the ICl A state give very sensitive information on the chemical bond [7].

This experiment is interesting too in the domain of laser frequency secondary standards. With proper frequency stabilization and control of the laser beam as well as of the stray fields, a large series of lines could be observed with linewidths well below 100 kHz. The reproducibility of these lines would be limited mostly by pressure shifts, probably in or near the kHz range. These lines are likely to provide good frequency standards in the red part of the visible spectrum.

We thank DGA DRET for supporting this project and we also thank Region Midi-Pyrénées for support of our laboratory. We have benefited from the help of several colleagues, especially F. Biraben, F. Nez, B. de Beauvoir, C.J. Bordé, F. Calvo, F.E. Cummings, R. Vetter and K. Janda. Finally, we are indebted toward C. Boone and F.W. Dalby for their very careful reading of the manuscript.

References

1. C.H. Townes, A.L. Shawlow, *Microwave Spectroscopy*, (McGraw-Hill, New York, 1955).
2. R. Bacis, M. Broyer, S. Churassy, J. Vergès, J. Vigué, J. Chem. Phys. **73**, 2641 (1980).
3. J.R. Johnson, T.J. Slotterback, D.W. Pratt, K.C. Janda, C.M. Western, J. Chem. Phys. **94**, 5661 (1990).
4. C.M. Western, T.J. Slotterback, J.R. Johnson, D.W. Pratt, K.C. Janda, J. Chem. Phys. **98**, 1826 (1993).
5. T.J. Slotterback, S.G. Clement, K.C. Janda, C.M. Western, J. Chem. Phys. **101**, 7221 (1994).
6. T.J. Slotterback. K.C. Janda, C.M. Western, J. Chem. Phys. **103**, 9125 (1995).
7. C.M. Western. W.S. Barney, S.G. Clement, T.J. Slotterback, K. Janda, Z. Phys. D **36**, 273 (1996).
8. S.J. Harris, W.C. Natzle, C.B. Moore, J. Chem. Phys. **70**, 4215 (1979).
9. J.A. Coxon, M.A. Wickramaaratchi, J. Mol. Spectrosc. **79**, 380 (1980).
10. J.A. Coxon, R.M. Gordon, M.A. Wickramaaratchi, J. Mol. Spectrosc. **79**, 363 (1980).
11. H.G. Hedderich, P.F. Bernath, G.A. McRae, J. Mol. Spectrosc. **115**, 384 (1992).
12. E. Herbst, W. Steinmetz, J. Chem. Phys. **56**, 5342 (1972).
13. M. Broyer, J. Vigué, J.C. Lehmann, J. Phys. (Paris) **39**, 591 (1978).
14. J.P. Pique, F. Hartmann, Phys. Rev. Lett. **52**, 267 (1984).
15. J.P. Pique, F. Hartmann, S. Churassy, R. Bacis, J. Phys. (Paris) **47**, 1917 (1986).
16. J.P. Pique, F. Hartmann, S. Churassy, R. Bacis, J. Phys. (Paris) **47**, 1909 (1986).
17. J. Vigué, M. Broyer, J.C. Lehmann, J. Phys. (Paris) **42**, 961 (1981).
18. M. Lamrini, R. Bacis, S. Churassy, P. Crozet, A.J. Ross, J. Chem. Phys. **100**, 8780 (1994).
19. J. Tellinghuisen, J. Chem. Phys. **106**, 1305 (1997).
20. F.E. Cummings. Ph. D. thesis, Harvard University, 1972.
21. G. Bazalgette, Ph. D. thesis, Université Paul Sabatier, 1997.
22. D.J. Seery, D. Britton, J. Phys. Chem. **68**, 2263 (1964).
23. P. Sulzer, K. Wieland, Helv. Phys. Acta **25**, 653 (1952).
24. K.P. Huber, G. Herzberg, *Molecular Spectra and Molecular Structure*, 2nd edn. (Van Nostrand Reinhold Company, New York, 1950).

25. F.E. Cummings, W. Klemperer, J. Chem. Phys. **60**, 2035 (1974).
26. A. Durand, J.C. Loison, J. Vigué, J. Chem. Phys. **106**, 477 (1997).
27. F. Biraben, P. Labastie, Opt. Commun. **41**, 49 (1982).
28. T.W. Hänsch, B. Couillaud, Opt. Commun. **35**, 441 (1980).
29. G. Camy, Ph. D. thesis, Université Paris-Nord, 1979.
30. J.L. Hall, S.A. Lee, Appl. Phys. Lett. **29**, 367 (1976).
31. J. Cachenaut, C. Man, P. Cerez, A. Brillet, F. Stoeckel, A. Jourdan, F. Hartmann, Rev. Phys. Appl. **14**, 685 (1979).
32. H. Kogelnick, T. Lines, Appl. Opt. **5**, 1550 (1966).
33. A. Durand, J.C. Loison, J. Vigué, J. Chem. Phys. **101**, 3514 (1994).
34. M. S. Sorem, A.L. Schawlow, Opt. Commun. **5**, 148 (1972).
35. T.G. Quinn, Metrologia **30**, 523 (1993/94).
36. K. Sengstock, U. Sterr, G. Hennig, D. Bettermann, J.H. Müller, W. Ertmer, Opt. Commun. **103**, 73 (1993).
37. K. Sengstock, U. Sterr, J.H. Muller, V. Rieger, D. Bettermann, W. Ertmer, Appl. Phys. B **59**, 99 (1994).
38. J.C. Bergquist, W.M. Itano, F. Elsner, M.G. Raizen, D.J. Wineland, *Single ion optical spectroscopy*, in *Light Induced Kinetic Effects on Atoms, Ions and Molecules*, edited by L. Moi, S. Gozzini, C. Cabbanini, E. Arimondo, F. Strumia, (ETS Editrice, Pisa, 1991).
39. A. Schenzle, R.G. Devoe, R.G. Brewer, Phys. Rev. A **25**, 2606 (1982).
40. J. Helmcke, S.A. Lee, J.L. Hall, Appl. Opt. **21**, 1686 (1982).
41. C.J. Bordé, G. Camy, B. Decomps, Phys. Rev. A **20**, 254 (1979).
42. A. Durand-Noyer, Ph. D. thesis, Université Paul Sabatier, 1995.
43. G. Birnbaum, Adv. Chem. Phys. **12**, 487 (1967).
44. A. Durand, J.C. Loison, G. Bazalgette, E. Gangler, F.W. Dalby, J. Vigué, Chem. Phys. **181**, 209 (1994).